

Hydrodynamic modeling of accretion onto stellar magnetospheres

I.A. Kryukov^{1,2}, N.V. Pogorelov^{1,2}, G.S. Bisnovatyi-Kogan³, U. Anzer², and G. Börner²

¹ Russian Academy of Sciences, Institute for Problems in Mechanics, Vernadskii Avenue 101-1, Moscow 117526, Russia (pgrlv@ipmnet.ru)

² Max-Planck-Institut für Astrophysik, Karl-Schwarzschild-Strasse 1, 85740 Garching bei München, Germany (ula,grb@mpa-garching.mpg.de)

³ Russian Academy of Sciences, Space Research Institute, Profsoyuznaya St., 84/32, Moscow 117810, Russia (kogan@mx.iki.rssi.ru)

Received 17 March 2000 / Accepted 22 September 2000

Abstract. A numerical investigation is performed of the accretion of slowly rotating matter onto a stellar magnetosphere. The shape of the magnetosphere is represented by an impermeable, contracted dipole magnetic field surface with polar holes. Depending on the governing parameters, both steady-state solutions with a system of discontinuities and unsteady flows with expanding shock waves can be obtained. Certain solutions exhibit extended outflow regions. The simulation is performed using a high-resolution finite volume numerical scheme and structured irregular grids adapted to the shape of the accreting body.

Key words: accretion, accretion disks – hydrodynamics – methods: numerical – stars: magnetic fields

1. Introduction

Accretion onto neutron stars and black holes gives the main energy supply in galactic X-ray sources. If the angular momentum of the matter provided by the massive companion star is sufficiently large, accretion occurs through a disk formed by the centrifugal forces. In this case, there exist two substantially different mechanisms which allow accreting matter to loose its angular momentum in the vicinity of the inner boundary of the accretion disk and fall onto the star. One of them is based on the classical turbulent viscosity model by Shakura (1972) and Shakura & Sunyaev (1973). Another mechanism is due to Sawada et al. (1986) who found out that spiral shocks originating inside the accretion disk are able to diminish the angular momentum of the matter to such an extent that the centrifugal forces cannot prevent its accretion on the star.

Another limit in the variety of accretion flows relates to accretion from a high-speed wind. If this wind is supersonic, a bow shock is forming near the black hole or near the stellar magnetosphere. Depending on the velocity of the incoming flow at infinity and on the cooling phenomena in the vicinity of the accretor, various accretion patterns can be obtained (see three-dimensional calculations by Ishii et al. 1993; Ruffert 1994). The existence of a steady-state solution for the wind accretion

flow is the subject of current discussions. Numerous unsteady patterns resulting in the formation of transient accretion disks (Shima et al. 1998) coexist with the self-similar (Bisnovatyi-Kogan et al. 1979) and numerical Newtonian (Pogorelov et al. 2000) and relativistic (Font & Ibañez 1998a, 1998b; Font et al. 1999) steady-state solutions.

Under high wind velocity conditions, the angular momentum of infalling matter is sometimes not sufficient for the accretion disk formation at distances of the Alfvén radius where the magnetic pressure of the star is in balance with the dynamic pressure of the gas, and approximately spherical free-fall onto the magnetosphere takes place, see the discussion by Illarionov & Sunyaev (1975), Cassen & Pettibone (1976), Shapiro & Lightman (1976), Arons & Lea (1980). This occurs in some binary X-ray sources with a massive companion star where long-periodic pulsars are observed (Nagase 1989; Börner et al. 1987; Bisnovatyi-Kogan 1991; Anzer & Börner 1995).

Without angular momentum, the flow pattern reduces to a purely spherically-symmetric one (Bondi 1952; Ruffert & Arnett 1994). Self-similar spherically-symmetric accretion in the gravitational field of a point mass was thoroughly investigated by Kazhdan & Murzina (1994) for the case of an adiabatic flow with a power-law density distribution far from the accreting center. They performed the analysis of various situations, starting from hydrostatic equilibrium to an arbitrary Mach number at infinity. One of the important results obtained by these authors is that the accretion pattern strongly depends on the boundary conditions at the center, namely, on the accretion rate at $R = 0$. The solutions can be subdivided into two groups. One group contains continuous, supersonic infall solutions (the Bondi solution belongs to this class). The other one contains various types of solutions with a shock wave expanding as $R_s \sim t^{2/3}$. These solutions for conditions fixed at infinity are characterized by the arbitrary position of the shock wave at a given time. This position can be determined uniquely only if we specify the nature of the infall near the center. This means that the shock wave is formed due to the presence of imaginary impermeable or partially impermeable surfaces at the origin. They decelerate the falling gas to subsonic velocities.

The paper of Kazhdan & Murzina (1994) gives us the guideline to what we might expect if the flow is not self-similar. In this case we must specify conditions both at the outer ($R = R_0$) and

at the inner ($R = R_*$) boundary. Let the flow be supersonic at $R = R_0$. In this case we must specify all quantities on this spherical surface. If ρ , p , and U are dimensionless density, pressure, and radial velocity in terms of ρ_0 , $\rho_0 U_0^2$, and U_0 , respectively, the conservation relations for a spherically-symmetric shockless flow of perfect polytropic gas are

$$\frac{U^2}{2} + \frac{a^2}{\gamma - 1} - \frac{S}{R} = \frac{1}{2} + \frac{1}{(\gamma - 1)M_0^2} - \frac{S}{R_0} \equiv h_{t0}, \quad (1)$$

$$\rho U = \frac{R_0^2}{R^2}, \quad (2)$$

$$\frac{p}{\rho^\gamma} = \frac{1}{\gamma M_0^2} \equiv s_0. \quad (3)$$

Here we introduced the Mach number $M_0 = U_0/a_0$, $a_0 = \sqrt{\gamma p_0/\rho_0}$, and $S = GM/U_0^2 R_*$ (γ is the polytropic index, M is the mass of the star, and G is the gravitation constant). Steady shockless solutions do not exist for arbitrary conditions on the outer boundary, even if the inner boundary allows free penetration.

For example, if the inner boundary ensures the maximum accretion rate ($\dot{M} = 4\pi R^2 \rho U$) attainable for the shockless flow which is at rest at infinity (the case of hydrostatic equilibrium), then, according to Bondi (1952), it has the sonic point at $R = R_B$ with

$$U_B^2 = a_B^2 = \frac{1}{2} \frac{S}{R_B}. \quad (4)$$

The conservation relations (1)–(3) at this point give

$$\frac{5 - 3\gamma}{4(\gamma - 1)} \frac{S}{R_B} = h_{t0}. \quad (5)$$

If we want to preset some supersonic flow at $R_0 < R_B$, it is necessary to assume that

$$0 < h_{t0} < \frac{5 - 3\gamma}{4(\gamma - 1)} \frac{S}{R_0}. \quad (6)$$

One can hardly expect any shockless supersonic accretion pattern originating from hydrostatic equilibrium at infinity if the total enthalpy lies without the interval (6).

If, for some reason, shockless accretion is not realized, then according to the self-similar solution by Kazhdan & Murzina (1994) a shock wave will originate at the inner boundary and propagate outward until it reaches the external boundary. Note that calculations with a subsonic inflow at $R = R_0$ are numerically much more difficult.

The situation becomes even more complicated if the inner boundary as a whole or some of its parts are not completely permeable. The problem in this case is at least two-dimensional and simple mathematical manipulations are no longer possible. For this reason we have to perform systematic numerical parametric studies. Bisnovatyi-Kogan & Pogorelov (1997) investigated the accretion of slowly rotating matter onto a gravitating center emphasizing the possibility of steady-state accretion patterns. For all quantities fixed at $R = R_0$, the dependence on the dimensionless parameter $S_r = GM/\omega_*^2 R_*^3$ was studied. Here

ω_* is the angular velocity which could be attained at the distance R_* from the axis of rotation under the assumption of constant angular momentum distribution. The cases corresponding to $1.5 \leq S_r \leq 250$ were considered.

Chen et al. (1997) dwelt on the accretion patterns with expanding shock waves. Those authors also performed calculations for $S_r < 1$. Igumenshchev et al. (1993) presented their results on the quasispherical accretion of matter onto a relativistic object with anisotropic X-ray luminosity and obtained the phenomenon of a hot gas outflow. Toropin et al. (1999) have recently calculated a quasi-spherical Bondi-like accretion onto a magnetic dipole. The study was performed using resistive magnetohydrodynamic (MHD) simulations in the axisymmetric case. The matter was assumed to have no angular momentum and the main results implied no rotation of the star. The authors specified supersonic Bondi solution at $R = R_0$. Note that this solution refers to a rather large accretion rate at $R = R_*$ and can be expected only at the early stages of accretion on the magnetic field of the star. This seems to be the reason why they obtained only one type of the accretion pattern which possesses an outward moving shock wave. Note also that the initial stage of the time-dependent accretion flow corresponds to small radiative cooling (large values of γ), which later becomes more efficient for optically thin plasma.

The model of accretion implemented numerically by Toropin et al. (1999) and in our paper corresponds to the scenario of Arons & Lea (1976). According to it, the plasma flow is initially decelerated by the star magnetosphere, with cusps forming in the polar regions (see Lipunov 1992). Later on, owing to the Rayleigh-Taylor instabilities which act in the equatorial region, clumps of plasma penetrate beneath the magnetopause and, threaded by the magnetic field, fall freely along the magnetic field lines onto the poles under the action of gravity. In the approach adopted by Toropin et al. (1999) the matter penetrates through the stellar magnetosphere owing to magnetic diffusion resulting from the finite conductivity of the plasma. This mechanism can result in the formation of an accretion picture which is quite different from what we expect in reality.

In our paper we choose another, although still simplified, approach which allows us to stay within a purely gas dynamic approximation of the problem. We assume that, on entering inside the magnetopause, the clumps of plasma are homogenized within a layer adjacent to the inner side of the initial magnetospheric surface and soon after that we again can consider the gas flow in the continuum approximation. Due to its complexity, for now this intermediate stage of the scenario is omitted and we investigate only the resulting flow. This flow occurs around some modified shape of the magnetosphere which is characterized by the presence of polar holes. The surface of the obtained magnetopause is impermeable for the accreting flow, whereas near the magnetic poles the matter can fall towards the star. These parts of the boundary are modeled by freely penetrable circular holes of specified radius. With this choice of the boundary we intend to simulate certain effects of the magnetic interaction. Outside the boundary we treat the flow as a purely gas dynamic process. Despite obvious simplifications, this model seems to be a nat-

ural initial step in the detailed study of the accretion process. Note in this connection that magnetohydrodynamic effects are mainly essential in description of the penetration process itself. The models governing this process are to be developed.

The paper is structured as follows. In Sect. 2 we state the mathematical problem and describe the dimensionless parameters governing it. Sect. 3 describes some specific features of the applied numerical method. In Sect. 4 we present various numerical results, and Sect. 5 gives the discussion.

2. Statement of the problem

The considerations given in the previous section allow us to perform the analysis on the basis of the numerical solution of the Euler gas dynamic equations. Suppose the flow pattern to be axisymmetric with the gravitating object placed at the origin of the coordinate system and with the rotation axis aligned with the z -axis (Fig. 1). The matter is assumed to be ideal and thermally perfect. By assuming the heat release/absorption processes to be polytropic we can write the caloric equation of state in the form

$$\varepsilon = \frac{p}{(\gamma - 1)\rho},$$

where ε is the internal energy per unit mass and γ is the polytropic index. The system of governing equations in the Cartesian coordinate system shown in Fig. 1 reads:

$$\frac{\partial \mathbf{U}}{\partial t} + \frac{\partial \mathbf{E}}{\partial x} + \frac{\partial \mathbf{G}}{\partial z} + \mathbf{H} = \mathbf{0}, \quad (7)$$

where

$$\mathbf{U} = [\rho, \rho u, \rho v, \rho w, e]^T, \quad (8)$$

$$\mathbf{E} = [\rho u, \rho u^2 + p, \rho uv, \rho uw, (e + p)u]^T \quad (9)$$

$$\mathbf{G} = [\rho w, \rho uw, \rho vw, \rho w^2 + p, (e + p)w]^T, \quad (10)$$

$$\mathbf{H} = \frac{\rho}{x} \begin{bmatrix} u \\ (u^2 - v^2) + S_r x \frac{\sin \theta}{R^2} \\ 2uv \\ uw + S_r x \frac{\cos \theta}{R^2} \\ \frac{(e + p)u}{\rho} + S_r x \frac{u \sin \theta + w \cos \theta}{R^2} \end{bmatrix} \quad (11)$$

The superscript T means transposing. In the above system $e = p/(\gamma - 1) + \rho(u^2 + v^2 + w^2)/2$ is the total energy per unit volume. We normalized the quantities of density, velocity, and pressure by $\rho_0, \omega_* R_*, \rho_0 \omega_*^2 R_*^2$, where R_* is the reference length defined by the formula approximating the solid portion of the contracted magnetosphere of the star (Elsner & Lamb 1976)

$$R_m = R_* \exp\left(\frac{\cos 2\phi}{2}\right); \quad \frac{\pi}{2} - \theta = \phi + \frac{1}{2} \sin 2\phi. \quad (12)$$

In the first quadrant one has $0 \leq \phi \leq \pi/2$. The angle θ is counted off the z -axis. It is clear that at $\theta = 0$, the polar distance of the magnetosphere is $R_p = R_*/\sqrt{e}$. At the equator,

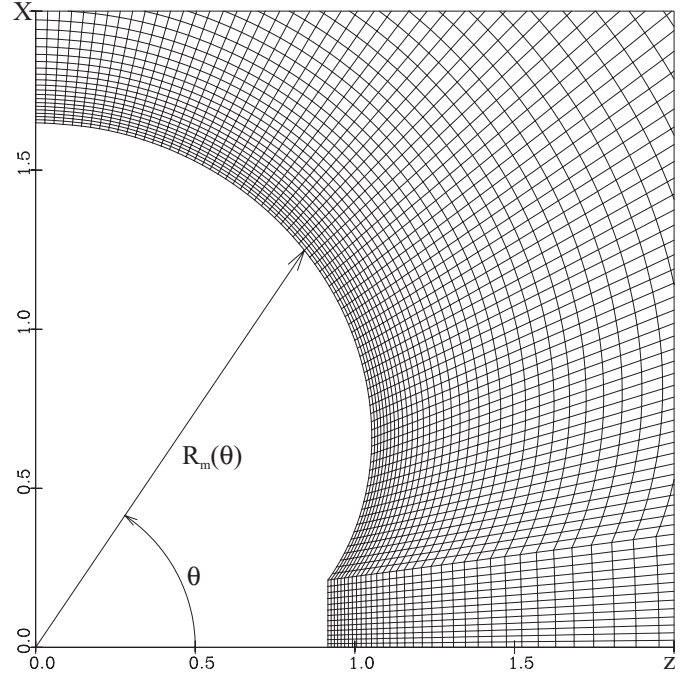


Fig. 1. Numerical grid and the profile of accreting magnetosphere.

$R_e = R_* \sqrt{e}$. We use this simplified formula in our calculations, since it adequately describes the shape of the magnetopause in a way sufficient for our qualitative studies. We have written out the dimensionless system for the general case in which the accreting matter possess some angular momentum at infinity. Modifications necessary in the case of the quasispherical accretion of matter without angular momentum will be given in Sect. 4.

We assume the inflow at $R = R_0$ to be supersonic. Thus, we must specify all quantities on the outer boundary. Taking into account this fact and inspecting the structure of the system (7)–(11), we arrive at the following set of dimensionless parameters of the problem: γ, M_0, S_r , and S , where $S = (U_{K*}/U_0)^2$. As previously noted, U_0 is the radial inflow velocity at $R = R_0$ and $U_{K*} = (GM/R_*)^{1/2}$ is the Keplerian velocity. By introducing these dimensionless parameters and initially assuming the flow to be spherically symmetric, we fix the values on the outer boundary as

$$\rho_0 = 1; \quad U_0 = -\left(\frac{S_r}{S}\right)^{1/2}; \quad p_0 = \frac{S_r}{\gamma S M_0^2}; \quad W_0 = 0,$$

where W_0 is the θ -component of the velocity vector.

Neglecting for the moment the velocity components in the angular directions, we can calculate the entropy function and the total enthalpy as

$$s_0 = \frac{p_0}{\rho_0^\gamma}; \quad h_{t0} = S_r \left[\frac{1}{S} \left(\frac{1}{(\gamma - 1)M_0^2} + \frac{1}{2} \right) - \frac{1}{R_0} \right].$$

We now choose the dimensionless R_0 to be 100 and introduce the following distribution of the angular velocity along the outer boundary:

$$\begin{cases} \omega = \frac{1}{x^2} = \frac{1}{R_0^2 \sin^2 \theta} & \text{if } x > 20 \\ \omega = 0.0025 & \text{if } x \leq 20 \end{cases}$$

The first interval here corresponds to the constant angular momentum and the second to the constant angular velocity distribution, respectively. The y -component v (normal to the plane of Fig. 1) of the velocity vector \mathbf{v} is then $v = \omega x$.

To modify the quantities of ρ_0 and p_0 at $R = R_0$, we assume $U(R_0, \theta) = U_0$ and $W(R_0, \theta) = 0$ and calculate the new values from the formulas

$$\frac{\gamma}{\gamma - 1} \frac{p_0}{\rho_0} + \frac{U_0^2}{2} + \frac{v_0^2}{2} - \frac{S_r}{R} = h_{t0}; \quad \frac{p_0}{\rho_0^\gamma} = s_0$$

Because of the symmetry of the problem, it suffices to seek solution only in the first quadrant. The conditions on the inner boundary are the following: nonpenetration is adopted for $\theta_* < \theta \leq \pi/2$, and absorbing boundary conditions are used for $0 \leq \theta \leq \theta_*$. The essence of these absorbing boundary conditions is described in Pogorelov & Semenov (1997). We use the quantity extrapolation at the supersonic exit $|w| > a$ and apply the relations in the rarefaction fan to accelerate the outflow velocity to the sonic value if $|w| < a$. These conditions give results nearly identical to those obtained with the “vacuum” boundary conditions by Hunt (1971) if the latter are used in the framework of the Godunov-type schemes (Toro 1997).

The initial conditions are believed to be not very important if we seek a steady-state solution. On the other hand, they are of crucial importance if we study transient phenomena.

3. Numerical method

For the numerical solution of the system (7)–(11) we use the hydrodynamic simulation method developed by Ivanov & Kryukov (1996). This method is based on the numerical scheme which provides high (second or third) order resolution of functions in the regions of their smoothness and preserves their monotonicity at discontinuities. This scheme is a modification of the Godunov scheme and can be attributed either to the TVD (total variation diminishing) or ENO (essentially nonoscillatory) classes depending on the implementation of the code modules. To find the fluxes through the computational cell interfaces, either the exact or some of the approximate solutions to the Riemann problem of the disintegration of an arbitrary discontinuity are used. In order to determine the values of the vector \mathbf{U} on the right- and left-hand sides of a cell interface, we use a substantially two-dimensional reconstruction procedure. The time integration is performed by the third-order Runge-Kutta method.

4. Simulation results

Our numerical results are subdivided into two groups. One of them deals with accretion of nonrotating gas onto the model

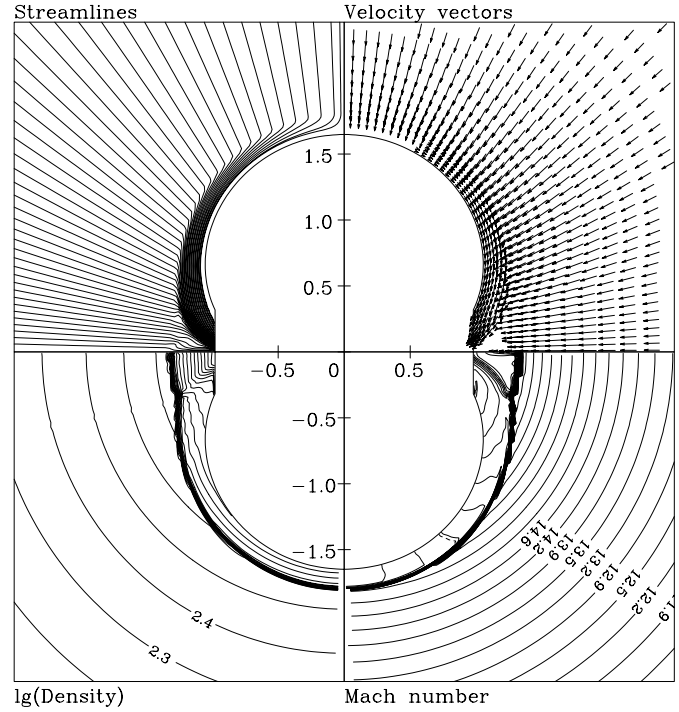


Fig. 2. Quasispherical accretion pattern for $S = 100$, $M_0 = 2$, $\gamma = 1.1$, and $d = 0.3$ ($|v|_{\max} = 145.3$).

magnetosphere. The other one concerns accretion of slowly rotating matter. In the former case, the y -component of the velocity vector \mathbf{v} and the corresponding equation for its determination vanish in the system of (7)–(11). If we normalize velocity and pressure by U_0 and $\rho_0 U_0^2$, respectively, the structure of the system remains unchanged if we substitute S_r by S in the source term.

4.1. Quasispherical accretion onto magnetosphere

In Fig. 2 we present the numerical results for the following parameters: $S = 100$, $M_0 = 2$, $\gamma = 1.1$, and $d = 0.3$ (the last parameter specifies the radius of the polar hole). The value of the polytropic index was chosen sufficiently small to account for the radiative cooling effects.

Note that the size of the holes in the adopted model is fully determined by the thickness of the penetration layer, that is, on the details of the Rayleigh-Taylor (interchange) instability of the magnetopause. Thus, the radius of the holes is a parameter of the problem. The depth of penetration cannot be smaller than the size of the plasma blobs occurring inside the layer. According to Arons & Lea (1976), the blob size is $(0.1\text{--}0.2) R_e$, or $0.15\text{--}0.3$ in our dimensionless units. This gives us a rough estimate for the variation range of d . The shape of the inner boundary in our case corresponds to the definition of plasmasphere introduced by Arons & Lea (1980).

Observational estimates of the polar hot spot cannot be done unambiguously since the observed beam is determined by the combination of a hot spot size and an angular size of the emission beam. Assuming the relation between the size of the hot spot

and Alfvénic radius (Baan & Treves 1973), we obtain the lower boundary of the angular radius of the hot spot of the order of 0.1 radian for the magnetic field (dipole component) $\sim 5 \times 10^{10}$ Gs (Sheffer et al. 1992; Baushev & Bisnovatyi-Kogan 1999; Scott et al. 2000).

The size of the polar holes was initially chosen fairly large, since we would like to be sure that the matter can be accreted at the rate prescribed by the external boundary conditions. Later we shall investigate the dependence of the accretion pattern on this size. We describe Fig. 2 in detail, since the subsequent figures have the same structure. In the first quadrant, we use arrows to show the velocity vectors. The size of each arrow is proportional to the magnitude of the velocity vector. In order to avoid misinterpreting, we limited the size of the vectors shown. The regions with small velocity manifest themselves as white zones free of arrows. The second quadrant shows the streamlines corresponding to the steady state obtained. The third quadrant contains the contours of constant density logarithms. In this plot we can distinguish the discontinuities which are likely to occur in the progress of flow deceleration by the impermeable surface of the magnetosphere. In the fourth quadrant, we show the contours of constant Mach numbers. Dotted lines represent the level $M = 1$.

In the adopted model, the flow is essentially the combination of a supersonic blunt body and a nozzle flow. It is therefore likely that a bow shock will appear in front of the impermeable portion of the magnetosphere. This shock decelerates the spherically-symmetric focusing stream of accreting matter to subsonic velocities. Such deceleration is caused by the nonpenetration boundary conditions. Note that there exists a stagnation point at $R = R_e$, $\theta = \pi/2$. In addition, the surface of the magnetosphere has a shape such that the radially oriented gravitation force always has a component directed along this surface towards the poles. The bow shock is finely resolved by the numerical scheme on the grid adapted to the magnetosphere surface. The streamline and especially the velocity vector pattern show the gas deflection at the magnetopause under the action of gravity. We can also distinguish a low-velocity zone adjacent to the stagnation point at the equator. The supersonic stream of matter can initially be freely accreted through the polar holes. In the course of time, however, as we approach the steady state, the freely falling column of matter surrounding the polar axis meets the convergent flow formed in the shock layer around the impermeable part of the magnetosphere. Collision of these two streams decelerates the former one, thus resulting in the origin of another shock. These two shocks form a combined bow shock around the magnetosphere. The resulting shock cannot generically be smooth and the derivative $R_{s\theta}$ of the shock surface $R = R_s(\theta)$ is discontinuous. It is clear that there must appear a third shock at this point. That is why, this point is called a triple point. We can see all these shocks in the density and Mach number contour plots. Their presence is also confirmed by the distribution of the lines $M = 1$ (the sonic lines). Note that the stream inside the shock layer, spreading over the magnetosphere surface in the equatorial region, soon becomes supersonic again. There exists another sonic line in

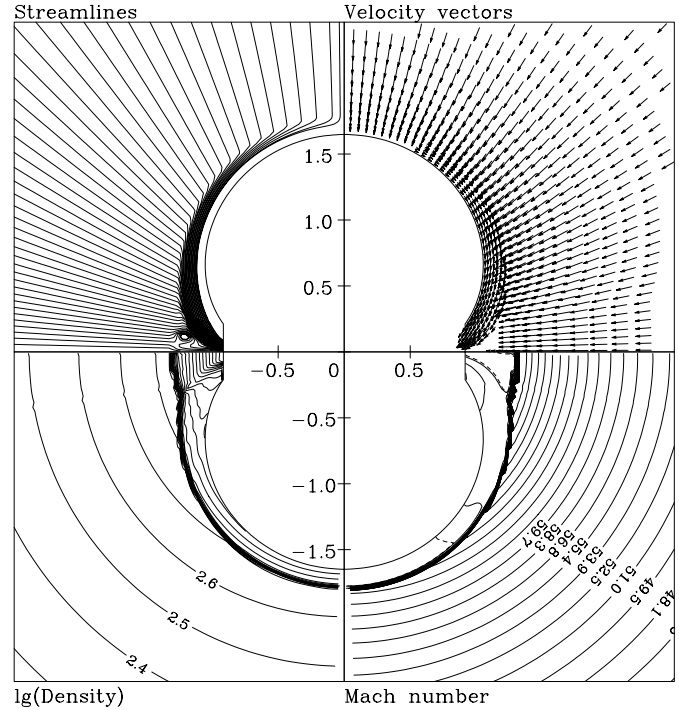


Fig. 3. Quasispherical accretion pattern for $S = 100$, $M_0 = 8$, $\gamma = 1.1$, and $d = 0.2$ ($|v|_{\max} = 149.0$).

the vicinity of the polar holes. On this line the gas in the blunt body shock layer decelerates to subsonic velocities again. This implies the existence of a shock wave. The last sonic line is not very well seen among the Mach lines in Fig. 2. One can easily distinguish it in Figs. 3 and 4, where we show the solution for $S = 100$, $M_0 = 8$, $\gamma = 1.1$, and $d = 0.2$ and 0.1 , respectively. In these figures, the slip line between the two portions of the flow passing through the different parts of the bow shock is also very well seen. It is apparent that this slip line originates at the triple point.

It is worth emphasizing, that for large values of the parameter S , that is, for strong gravitation the influence of the Mach number M_0 on the flow pattern becomes rather weak, since the matter is rapidly accelerating at large distances from the star and acquires hypersonic values ahead of the bow shock.

Note that the streamlines oriented along the polar axis can find their way to the star only through a very narrow hole near this axis. The main portion of accreting matter is supplied by the supersonic stream formed in the narrow shock layer around the impermeable part of the magnetosphere. This, in fact, means that accretion of initially almost spherically symmetric flow occurs in a way consistent with that predicted by Arons & Lea (1976). It is interesting that even a very narrow polar hole with $d = 0.1$ (Fig. 4) permits the accretion rate prescribed on the outer boundary. We can conclude that a steady-state accretion pattern can be realized along with the highly unsteady results predicted by Kazhdan & Murzina (1994) and obtained numerically by Chen et al. (1997) and Toropin et al. (1999). It is also worth mentioning that smaller sizes of the holes result in larger bow shock stand-off distances. This is quite reasonable, since in the

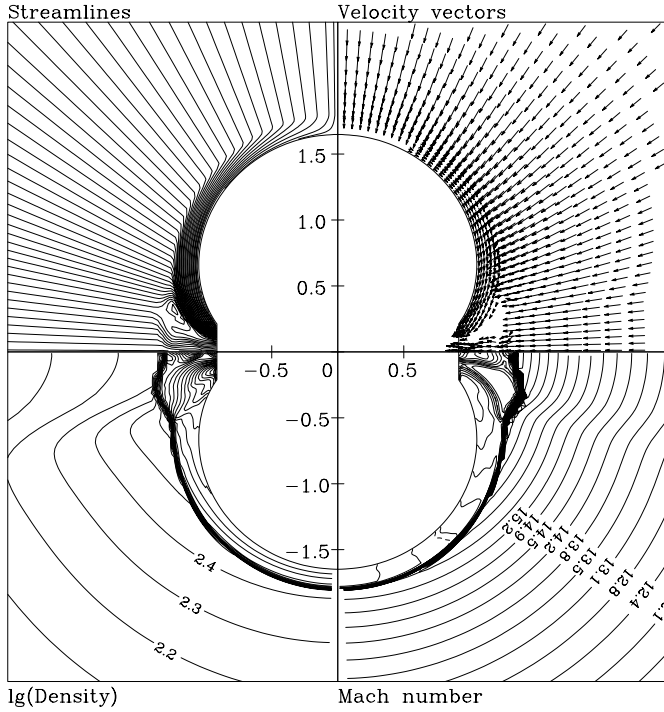


Fig. 10. Accretion pattern for $S = 100$, $S_r = 250$, $M_0 = 2$, $\gamma = 1.1$, and $d = 0.2$ ($|v|_{\max} = 358.3$).

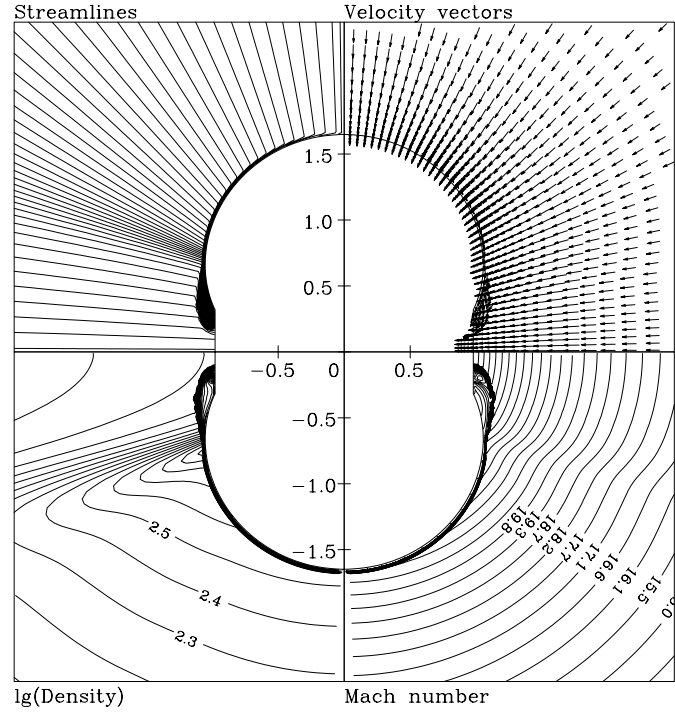


Fig. 12. Accretion pattern for $S = 100$, $S_r = 40$, $M_0 = 2$, $\gamma = 1.01$, and $d = 0.3$ ($|v|_{\max} = 80.11$).

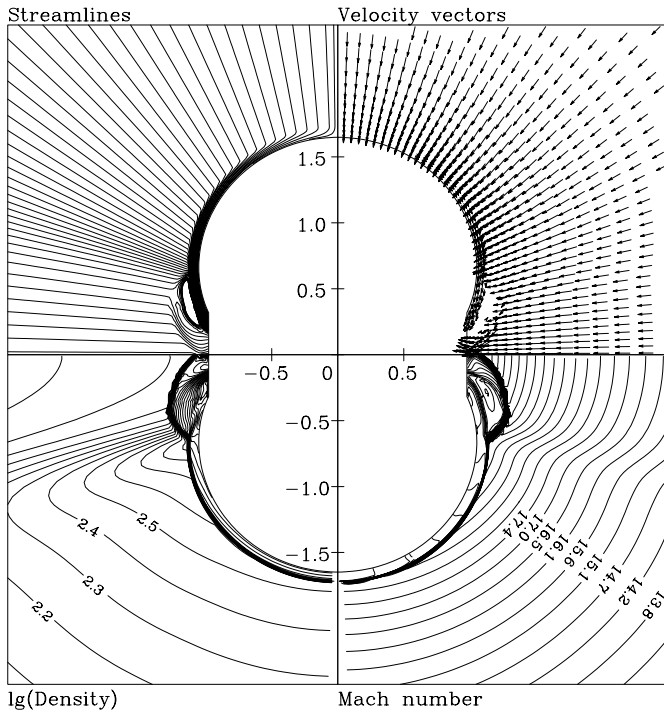


Fig. 11. Accretion pattern for $S = 100$, $S_r = 60$, $M_0 = 2$, $\gamma = 1.05$, and $d = 0.3$ ($|v|_{\max} = 106.5$).

to development of a growing magnetosphere accompanied by a bow shock propagation outward. A steady-state solution cannot be obtained in this case. In Fig. 11 we show one of the solutions on the boundary between the steady-state and nonstationary so-

lutions. The flow presented corresponds to $S_r = 60$, $\gamma = 1.05$, and $d = 0.3$. The pattern is substantially different in this case. The triple point moves farther from the rotation axis and a low-velocity circulation zone originates behind the portion of the bow shock closer to the rotation axis (see the streamline and velocity vector distributions). The bow shock stand-off distance starts increasing right above the triple point, attains a maximum, and decreases to a rather small value at the rotation axis. The flow restructuring allows a large portion of the radially falling gas to be accreted avoiding preliminary compression in the shock layer near the impermeable surface of the magnetosphere. This permits us to obtain a steady-state solution. Smaller values of γ increase the compressibility of the falling matter which is highly compressed in the shock layer, as seen from the streamline distribution in Fig. 12 which corresponds to $S_r = 40$, $\gamma = 1.01$, and $d = 0.3$. For larger cooling effects, there appears a portion of matter around the symmetry axis which is accreted at a supersonic speed without any shock. Thus, the accretion pattern becomes qualitatively different in this case. It also turns out that a certain portion of the bow shock is intersected at rather acute angles. Decreasing the holes will lead to a solution with a divergent bow shock. We can see the dynamics of the accreting pattern in Figs. 13 and 14 which correspond to $S_r = 100$, $\gamma = 1.01$, and $d = 0.2$ and 0.1 , respectively. The solution shown in Fig. 13 represents a steady accretion with a very thin shock layer, owing to high compressibility of the matter at $\gamma = 1.01$. Narrow polar holes cannot ensure sufficiently high accretion rates and the matter starts accumulating around the magnetosphere. This finally results in an unsteady solution with the bow shock moving towards the outer boundary (Fig. 14).

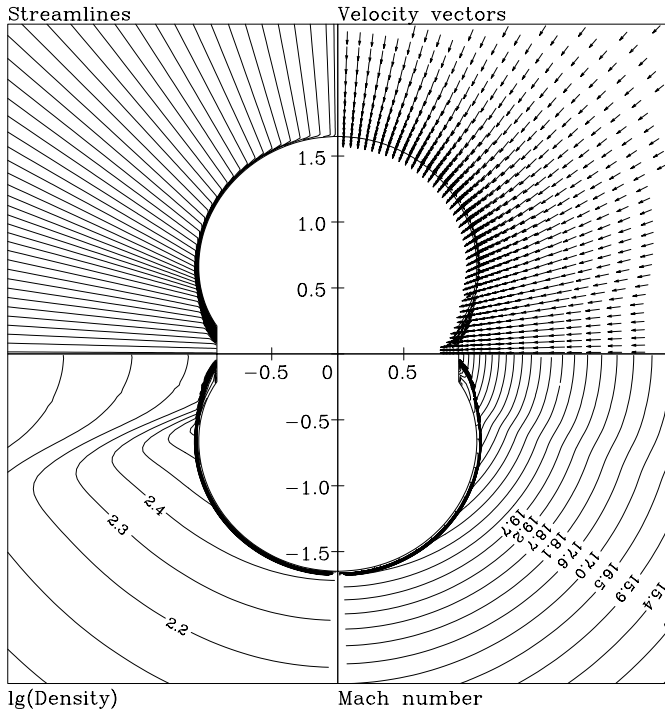


Fig. 13. Accretion pattern for $S = 100$, $S_r = 100$, $M_0 = 2$, $\gamma = 1.01$, and $d = 0.2$ ($|v|_{\max} = 213.1$).

It is important to note that the velocity of its propagation can sometimes be so large that the radial component of the velocity vector behind the shock becomes positive. This can be interpreted as an explosion-like formation of a gas cloud around the star.

5. Discussion

We have obtained steady-state numerical solutions for the quasi-spherical accretion of matter onto the model magnetosphere of a star. In our models we use a specially designed inner boundary for the flow region which is intended to simulate the effects of the stellar magnetosphere. The shape of the magnetosphere in the accepted model is characterized by the presence of an impermeable surface represented by a contracted dipole magnetic field line and of holes in the polar regions. These holes can be interpreted as a result of the cusp disintegration caused by the Rayleigh-Taylor instability of the zero-approximation (totally impermeable) magnetospheric surface occurring in its equatorial regions. We also assumed that the magnetic axis and the rotation axis are aligned. This then allows us to use a simple gas dynamic approach in a two-dimensional geometry. We showed that steady solutions can exist for boundary conditions consistent with the accretion ability of the polar holes. This occurs for low values of the polytropic index, small rotation rates of the gas, and sufficiently large polar holes. These flows show a stationary shock front around the magnetosphere. Our results supplement unsteady solutions with expanding shock waves obtained by various authors.

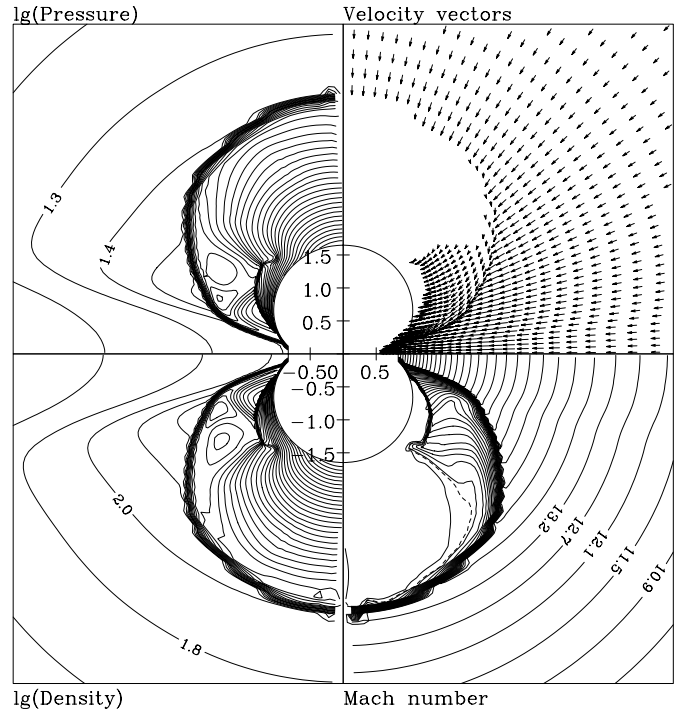


Fig. 14. Accretion pattern for $S = 100$, $S_r = 100$, $M_0 = 2$, $\gamma = 1.01$, and $d = 0.1$ ($|v|_{\max} = 235.0$).

The model of a stationary magnetosphere used in our calculations is overidealized in some aspects. The main simplification is in ignoring the details of the magnetic interaction of the star with the accretion flow. Our simplification, however, in contrast with that adopted by Toropin et al. (1999), represents another limit of the realistic phenomenon. The latter model implies that accretion can occur only due to the plasma diffusion through the magnetic field lines of the magnetosphere. To account for larger accretion rates, one must adopt in this case higher electric resistivity of accreting matter. In our approach, we choose another limit of a highly unsteady accretion process launched by the instability of the stellar magnetosphere. In doing so, we assume that some averaged stream of plasma originates beneath the zero-order impermeable magnetopause, thus reducing the problem to a purely hydrodynamic accretion through the holes opening in the vicinity of the polar cusps. One can argue which model is closer to reality. To improve both models, we must take into account physical details of the plasma penetration beneath the magnetopause. More detailed consideration of the radiative cooling effects will also be highly favorable, since it would affect the actual mass accretion rate due to the obvious dependence of cooling on the matter density. For this reason, we consider our present calculations as a starting point of more complex MHD simulations.

The assumption that the rotation axis of the star and/or of the accreting gas are aligned with the magnetic axis is not very realistic. All stellar X-ray sources which are observed as pulsars require a finite inclination angle between these axes. The problem in this case becomes fully three-dimensional. In our calculations we neglected the development of the penetration

process beneath the magnetosphere occurring in its equatorial region according to Arons & Lea (1976). In this case the flow pattern would be much more complicated, consisting of several subsonic and supersonic regions with the formation of shocks around the magnetosphere as well as near the stellar surface. This is the subject of a future investigation. Nevertheless, even our two-dimensional symmetric calculations can describe some of the basic features of the wind accretion onto magnetized stars. On the other hand, one has to be aware that realistic treatment will require the study of the fully three-dimensional configurations.

Another important physical feature of the accretion phenomenon is connected with the radiative energy losses increasing as we approach the inner boundary. They lead to merging of the accreting matter with the matter of the star and to formation of standing shocks close to the stellar or magnetospheric surfaces. The steady-state position of these shocks will be determined by the radiative energy losses behind the shock.

Acknowledgements. I.A.K and N.V.P. are grateful to Max-Planck-Institut für Astrophysik in Garching bei München for hospitality. Performing this work, G.S.B.-K., A.I.K., and N.V.P. were partially supported by the Russian Foundation of Basic Research under Grant No. 98-01-00352.

References

- Anzer U., Börner G., 1995, *A&A*, 299, 62
 Arons J., Lea S.M., 1976, *ApJ*, 207, 914
 Arons J., Lea S.M., 1980, *ApJ*, 235, 1016
 Baan W., Treves A., 1973, *A&A*, 22, 421
 Baushev A.V., Bisnovaty-Kogan G.S., 1999, *Astron. Rep.*, 43, 241
 Bisnovaty-Kogan G.S., 1991, *A&A*, 245, 528
 Bisnovaty-Kogan G.S., Pogorelov N.V., 1997, *Astron. Astrophys. Trans.*, 12, 263
 Bisnovaty-Kogan G.S., Kazhdan Ya.M., Klypin A.A., Lutskii A.E., Shakura N.I., 1979, *SvA*, 23, 201
 Börner G., Hayakawa S., Nagase F., Anzer U., 1987, *A&A*, 182, 63
 Bondi H., 1952, *MNRAS*, 112, 195
 Cassen P., Pettibone D., 1976, *ApJ*, 208, 500
 Chen X., Taam R.E., Abramowicz M.A., Igumenshchev I.V., 1997, *MNRAS*, 285, 439
 Elsner R.F., Lamb F.K., 1976, *ApJ*, 215, 897
 Font J.A., Ibañez J.M., 1998a, *ApJ*, 494, 297
 Font J.A., Ibañez J.M., 1998b, *MNRAS*, 298, 835
 Font J.A., Ibañez J.M., Papadopoulos P., 1999, *MNRAS*, 305, 920
 Hunt R., 1971, *MNRAS*, 154, 141
 Igumenshchev I.V., Illarionov A.F., Kompaneets D.A., 1993, *MNRAS*, 260, 727
 Illarionov A.F., Sunyaev R.A., 1975, *A&A*, 39, 185
 Ishii T., Matsuda T., Shima E., Livio M., Anzer U., Börner G., 1993, *ApJ*, 404, 706
 Ivanov I.E., Kryukov I.A., 1996, *Matematicheskoe Modelirovanie [Mathematical Modeling]*, 8, No. 6, 47 [in Russian]
 Kazhdan Ya.M., Murzina M., 1994, *MNRAS*, 270, 351
 Lipunov V.M., 1992, *Astrophysics of Neutron Stars*, Springer, Berlin
 Nagase F., 1989, *PASJ*, 41, 1
 Pogorelov N.V., Semenov A.Yu., 1997, *A&A*, 321, 330
 Pogorelov N.V., Ohsugi Y., Matsuda T., 2000, *MNRAS*, 313, 198
 Ruffert M., 1994, *ApJ*, 427, 342
 Ruffert M., Arnett, D., 1994, *ApJ*, 427, 351
 Sawada K., Matsuda T., Hachisu I., 1986, *MNRAS*, 219, 75
 Scott D.M., Leahy D.A., Wilson R.B., 2000, *astro-ph/0002327*
 Shakura N.I., 1972, *Astron. Zh.*, 49, 921
 Shakura N.I., Sunyaev R.A., 1973, *A&A*, 24, 337
 Shapiro S.L., Lightman A., 1976, *ApJ*, 204, 555
 Sheffer E., Kopaeva I.F., Averintsev M.B., et al., 1992, *SvA*, 36, 41
 Shima E., Matsuda T., Anzer U., Börner G., Boffin H.M.J., 1998, *A&A*, 337, 311
 Toro E.F., 1997, *Riemann Solvers and Numerical Methods for Fluid Dynamics – A Practical Introduction*, Springer, Berlin
 Toropin Yu.M., Toropina O.D., Savelyev V.V., et al., 1999, *ApJ*, 517, 906